Fig. 3 Piezoelectric sensors with (a) current amplifier and (b) charge amplifier

dielectric matrix, and where the external mechanical force $\{\boldsymbol{f}_i\}$ and the electric charge $\{\boldsymbol{g}_i\}$ are defined as

$$\{\boldsymbol{f}_i\} = \int_V [\boldsymbol{N}_u]^{\mathrm{T}}[\boldsymbol{P}_{\mathrm{b}}]\,\mathrm{d}V + \int_{S_1}\int_V [\boldsymbol{N}_u]^{\mathrm{T}}\{\boldsymbol{P}_s\}\,\mathrm{d}\boldsymbol{S} + [\boldsymbol{N}_u]^{\mathrm{T}}\{\boldsymbol{P}_c\} \tag{11a}$$

$$\{\boldsymbol{g}_i\} = -\int_{S_2} [\boldsymbol{N}_\phi]^{\mathrm{T}}\sigma\,\mathrm{d}V - [\boldsymbol{N}_\phi]^{\mathrm{T}}Q \tag{11b}$$

In the above equations ρ is the mass density, P_{b}, P_{s}, and P_{c} are body forces, surface forces, and point forces applied on the structure, respectively, and Q is the applied concentrated electric charge. The shape functions $[\boldsymbol{N}_u]$, $\{\boldsymbol{N}_\varphi\}$ are related to the displacement field $\{u\}$ and the electric potential ϕ over an element, and $[\boldsymbol{B}_u]$ and $[\boldsymbol{B}_\varphi]$ are their shape function derivatives, respectively.

The numerical results presented in this article are obtained using the ANSYS finite-element program [**20**], which supports direct coupling field analysis. In this study, the eight-node element SOLID5 is used to model the piezoelectric strips and the 3D element SOLID45 is used to model the structure.

4 CRACK DETECTION SIMULATIONS FOR OSCILLATORY MECHANICAL LOADS

Case of static loads

A numerical simulation was first performed in the case of static mechanical loads for a cantilevered aluminium beam (of length 600 mm, width 20 mm, and 5 mm in thickness) with a normal static force of 2 N acting at the free end. The typical variation with the crack location of the induced voltage difference (representing the output of a sensor pair located at 280 mm from the fixed end) is illustrated in Fig. 4.

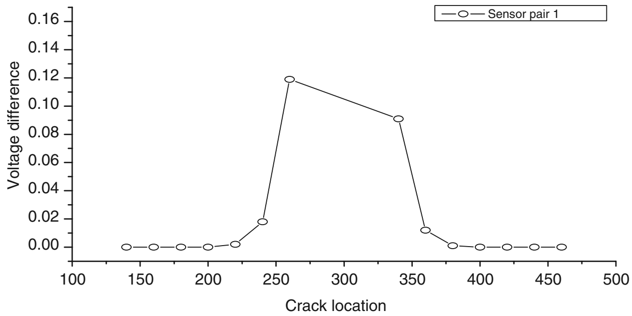

Fig. 4 Typical variation of the induced voltage difference with the crack location for static loads

One can notice that the voltage difference reduces substantially with the increase in the distance between the piezoelectric strip sensor pair and the crack, which indicates that the sensitivity of the crack detection method in the case of static mechanical loads is not good enough. This is substantially improved when flexural oscillations of the structure are used instead of static bending.

4.1 Results of harmonic analysis

This section examines the local strain changes measured by the piezoelectric sensors when the structure undergoes forced vibration, which may be generated by piezoelectric actuators.

The structural model used for the frequency domain analysis, shown in Fig. 5, is the same cantilevered aluminium plate of length 600 mm, width 20 mm, and 5 mm in thickness. Forced flexural oscillations of the structures are generated by a pair of two piezoelectric strip actuators (of length 40 mm and located at 480 mm from the fixed end) bonded on the opposite faces of the structure, which are submitted to oscillatory voltage excitations defined in the form

$$V = V_0 \sin(2\pi f t) \tag{12}$$

where V_0 is the voltage amplitude and f is the frequency of voltage oscillations. The amplitude of the voltage excitation V_0 used in the numerical simulations was 100 V and the frequency of oscillation, f, varied from 0 to 800 Hz in steps of 10 Hz.

Two pairs of piezoelectric strip sensors bonded on the opposite sides of the structure at 280 mm (pair 1) and 80 mm (pair 2) have been used to measure the difference between the strains on the opposite faces of the structure.

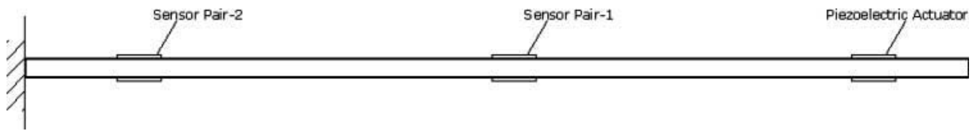

Fig. 5 Configuration of the plate used for harmonic analysis

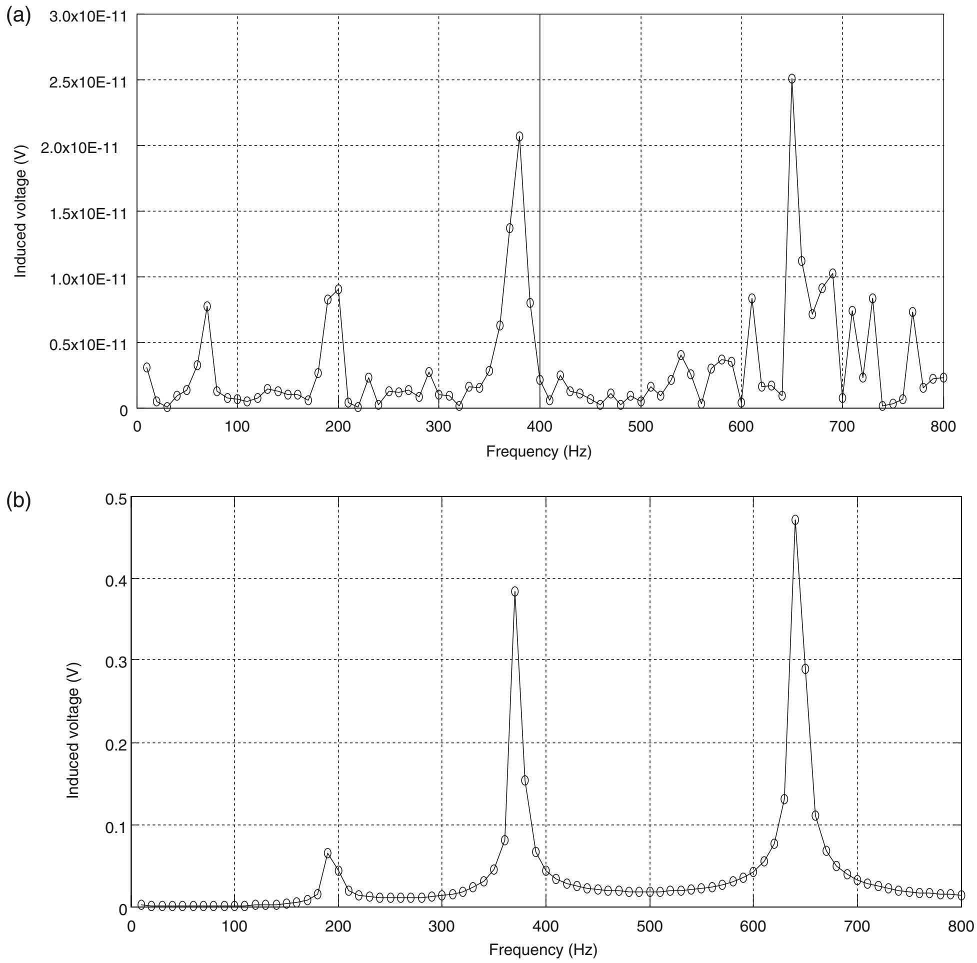

Fig. 6 Harmonic analysis. Typical variation of the voltage difference of the sensor pair, located at 80 mm from the fixed end, with the excitation frequency of the actuator: (a) in the absence of a crack and (b) when there is a crack located at 130 mm from the fixed end

The results of the numerical simulations using the modal analysis for the frequency sweep between 0 and 800 Hz are shown in Fig. 6. In the absence of a crack, there is practically no voltage difference between the upper and lower sensors of a pair (the order of magnitude is 10^{-11} V), as shown in Fig. 6(a). When there is a crack in the structure, the typical voltage difference measured by the sensor pair 2 (located at 80 mm from the fixed end) is illustrated in Fig. 6(b) for a crack located at 130 mm from the fixed end. This typical induced voltage difference displays two important peaks which appear at frequencies that are close to the natural frequencies corresponding to the sixth and eighth modal shapes of the plate (illustrated in Fig. 7), which are indicated in Table 1. These peaks are large enough to be detected, indicating thus the presence of a crack in the structure.

As a comment, one can notice from Table 1 that the differences between the natural frequencies of the undamaged beam and the cracked beam are very small, which makes the task to detect the presence of a crack in the structure by measuring the changes in the natural frequencies very difficult.

4.2 Results of time-dependent analysis

The time-dependent analysis is performed for a cantilevered beam (of length 400 mm, width 10 mm, and

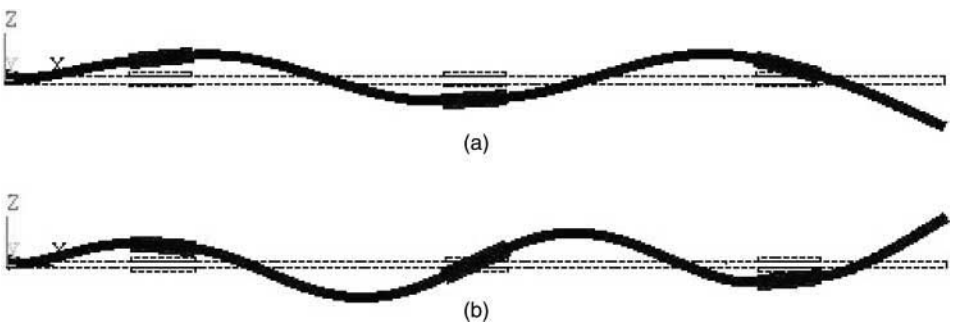

Fig. 7 (a) The sixth modal shape of the plate and (b) the eighth modal shape of the plate

Table 1 Comparison between the natural frequencies of undamaged and cracked plates

	Natural frequency (Hz)			
		Crack location on the damaged plate		
Mode	Undamaged plate	130 (mm)	180 (mm)	360 (mm)
1	10.532	10.503	10.507	10.528
2	40.233	40.194	40.200	40.228
3	65.857	65.832	65.809	65.551
4	194.110	193.59	193.690	193.800
5	254.200	254.18	254.140	254.930
6	374.821	373.66	374.590	374.660
7	524.783	524.56	524.570	524.700
8	645.861	644.52	645.620	644.900
9	745.920	745.21	745.230	745.400

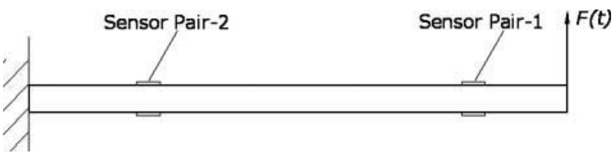

Fig. 8 Beam configuration for time-dependent structural analysis

thickness 10 mm) subjected to a time dependent normal force $F(t) = F_0 \sin(2\pi ft)$ acting at the free extremity. The configuration of the system is shown in Fig. 8, in which the locations of sensor pairs are varied in order to modify the distance between the crack and the sensors.

The effect of the distance between the sensor and the crack has been first evaluated (by changing the location of the sensor pair) and the results are shown in Fig. 9. It was found that when the distance is small, the shape of the voltage difference is more asymmetric and the amplitude of the voltage difference is larger. For larger distances, the voltage difference becomes symmetric and its amplitude becomes smaller.

The effect of the excitation frequency was also investigated. The lowest excitation frequency is chosen as 5 per cent of the first natural frequency of the beam without crack (the difference between the natural frequencies of the beam with or without cracks is very small, as shown in Table 1). The results shown in Fig. 10 indicate a slight increase of the voltage difference with the increase in the excitation frequency. However, considering the form of the voltage output variation in time (and the fact that in some cases of higher frequencies noise-like components might be

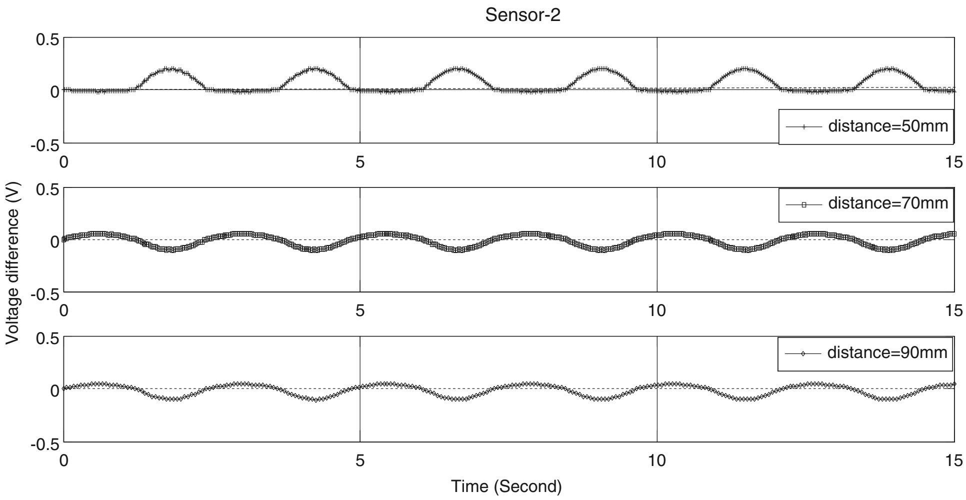

Fig. 9 Time-dependent analysis. Effect of the distance between the crack and the sensor. Results for three distances: 50, 70, and 90 mm

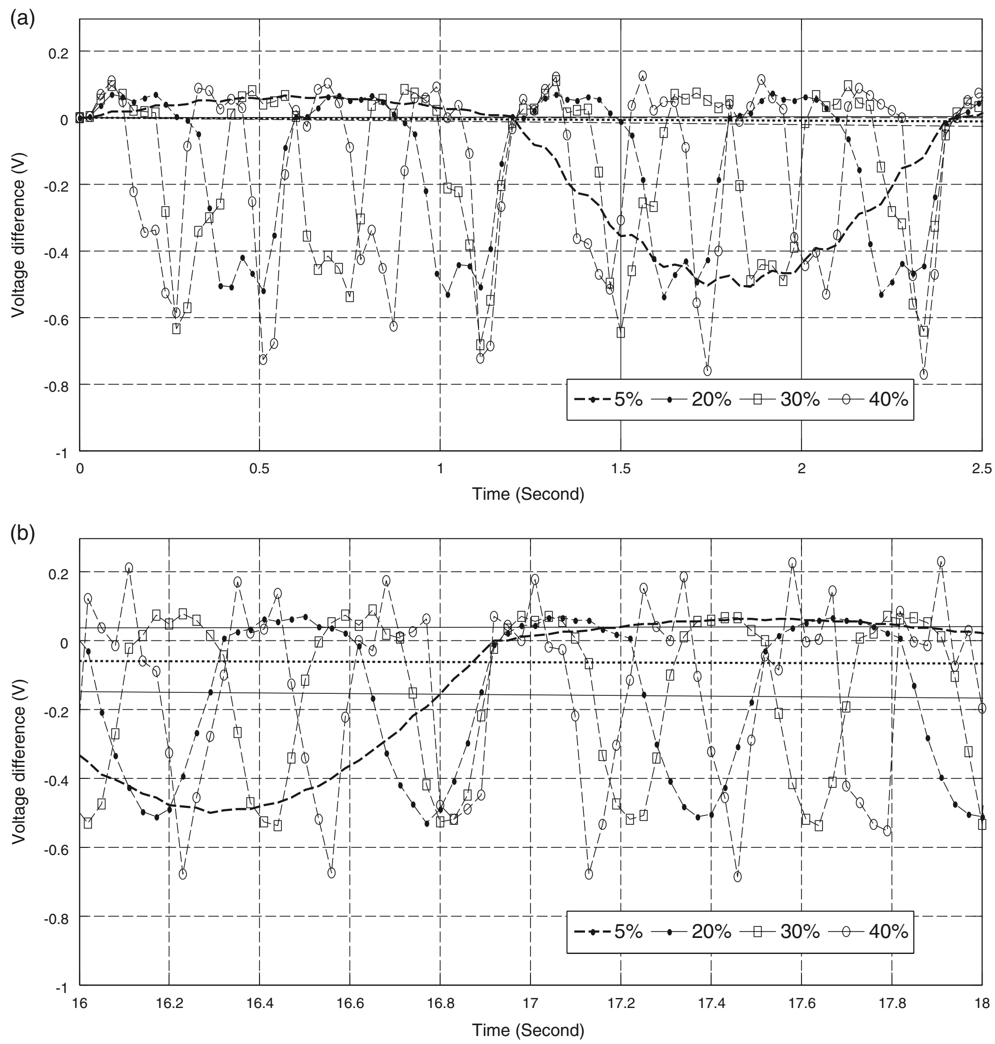

Fig. 10 Time-dependent analysis. Effect of the excitation frequency in the range of 5–40 per cent of the lowest natural frequency of the beam for a crack located at 300 mm from the fixed end. Results for: (a) $t \in [0,\ 2.5\,\text{s}]$, and (b) $t \in [16\,\text{s},\ 18\,\text{s}]$

also present), it is preferable to use for crack detection a lower forcing frequency, such as 5 per cent of the lowest natural frequency of the system, in which case the presence of the crack is very clearly indicated by the voltage difference output.

The effect of the crack depth on the induced voltage difference is shown in Fig. 11, which illustrates the results obtained for various values of the crack depth: 10 per cent, 25 per cent, and 37.5 per cent of the beam thickness. As expected, the voltage difference increases with the increase of the crack depth.

5 CRACK DETECTION SIMULATIONS FOR WING STRUCTURES SUBJECTED TO AERODYNAMIC LOADS

In this study, a rectangular wing with a crack is modelled by a plate of length (or semispan) $b = 2000$ mm, width (or chord) $c = 500$ mm, and thickness of 20 mm, which is fixed at one end, as shown in Fig. 12. Two pairs of piezoelectric strip sensors of length $\mathrm{p}l = 20$ mm, width $\mathrm{p}w = 120$ mm, and thickness 1 mm are bonded on this wing-like structure.

The numerical simulations consider the effect of a structural crack of depth 2 mm (representing 10 per cent of the plate thickness) and of various lengths, $l = 60$, 110, 160, 210, 260, 310, 360, 410, and 460 mm. Two positions have been considered for the crack on the wing: at cx $= 600$ mm and cx $= 1600$ mm from the fixed end.

Different locations of the piezoelectric sensor pairs have been considered along the plate length (or wing span) in order to vary the distance between the crack and the sensor pairs.

The steady and unsteady aerodynamic loads are computed in this analysis using a boundary element (panel) method developed in-house by the authors.

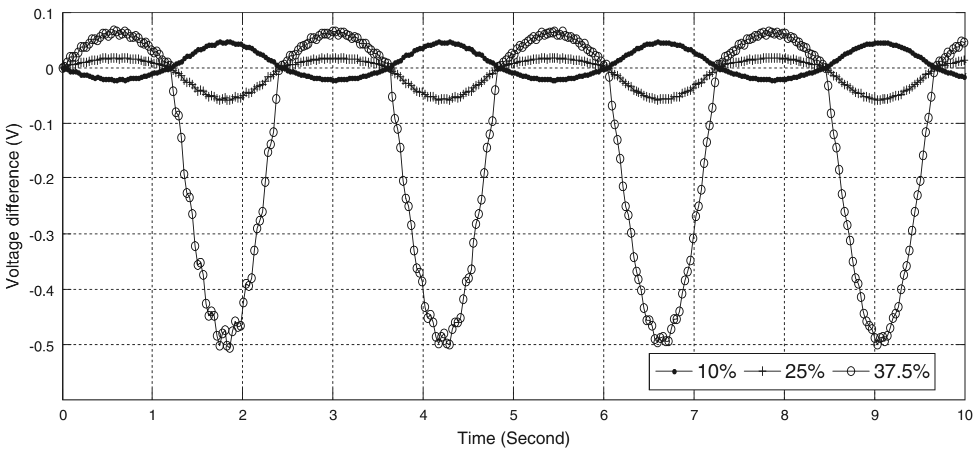

Fig. 11 Time-dependent analysis. Effect of the crack depth

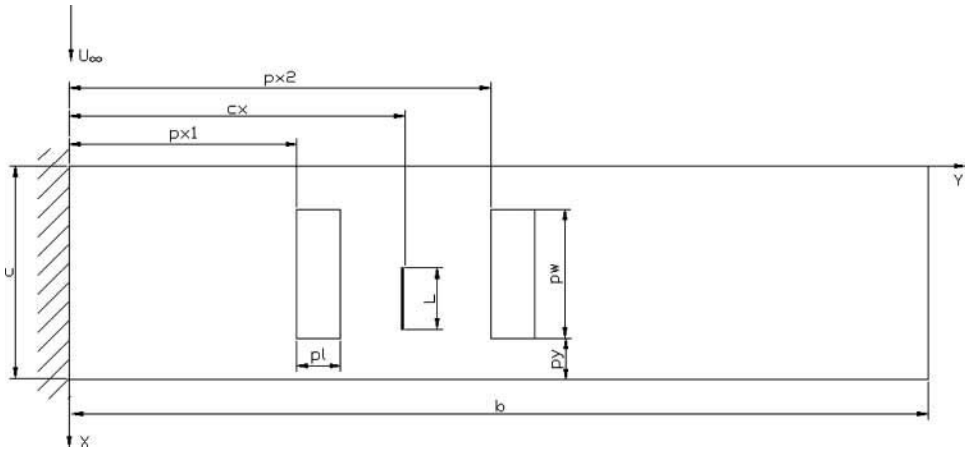

Fig. 12 Configuration of the crack detection system on a rectangular wing

In this case, the wing-like structure subjected to unsteady or steady loads has both flexural and torsional deformations. The deformation due to bending is represented by a curvature of the structure in the plane $y - z$, and the deformation due to the torsion is represented by a curvature of the structure in the plane $x - z$; thus the opposite sides of the structure will have different signs of strains: positive on one side (extension) and negative on the other side (compression). Hence, the deformation in torsion can contribute also to the crack detection, especially when the crack is not aligned in the chord direction. To maximize the sensitivity of the crack detection, one can use piezoelectric strips polarized in the wing span direction (for the flexural deformations) in conjunction with piezoelectric strips polarized in the chord direction (for the deformation in torsion), as used in reference [**17**] for the control of aeroelastic oscillations. In this feasibility study of the proposed detection method, however, no piezoelectric strips polarized in the chord direction are considered.

5.1 Results for cracked wing structures subjected to steady aerodynamic loads

The wing is considered to be placed in a steady uniform flow with a velocity of 75 m/s at an incidence $\alpha = 5°$. The crack is assumed to be situated at 600 mm from the fixed end. The length of the crack is varied between 60 and 460 mm, in order to evaluate the effect of the crack length. The piezoelectric sensors are located at 30 mm and at 50 mm distance from the crack, respectively, in order to evaluate the effect of the distance between the sensor and the crack. The results of the numerical simulations are shown in Figs 13 and 14.

As shown in Fig. 13, the voltage difference increases with the crack length. When the piezoelectric sensor pair is located near the crack, the voltage difference can be large.

Typical variation of the detection sensitivity with the distance between the sensor and the crack is shown in Fig. 14 for the cases when the crack is located at

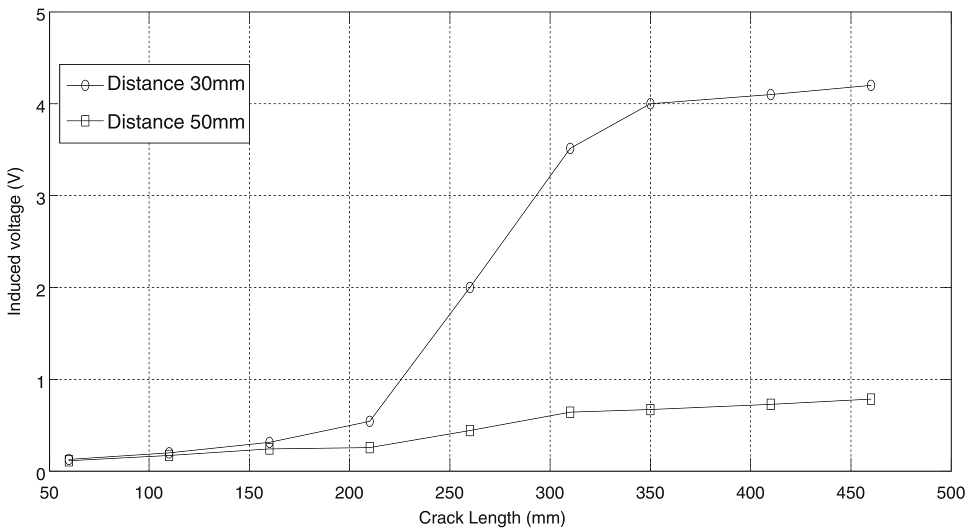

Fig. 13 Wing structure subjected to steady aerodynamic loads: typical voltage difference variation with the crack length for two distances between the sensor and the crack: 30 and 50 mm

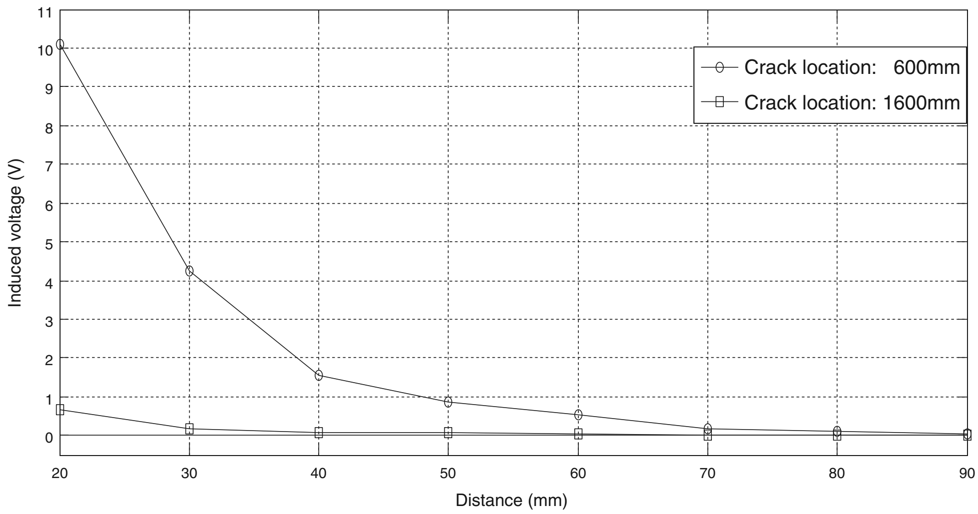

Fig. 14 Wing structure subjected to steady aerodynamic loads: typical voltage difference variation with the distance between the crack and the sensor pair for two crack locations

600 mm or at 1600 mm from the fixed edge of the plate (the crack length was 460 mm).

One can notice that voltage difference output decreases significantly with the distance between the crack and the sensor pair for both crack locations (although the voltage output values are different). This suggests that the steady lift forces acting on the wing structure cannot be used efficiently for crack detection (a similar conclusion was obtained in the case of static mechanical loads). By contrast, the unsteady aerodynamic loads acting on an oscillating wing structure are more efficient for the crack detection, as shown in the following.

5.2 Results for cracked wing structures subjected to unsteady aerodynamic loads

In this study, the wing is placed in a steady uniform flow with a velocity of 75 m/s and is assumed to execute oscillatory pitching rotations during which the angle of attack varies with time as $\alpha \sin(2\pi ft)$.

The effect of the crack location is shown in Fig. 15 for two locations of the crack ($cx = 600$ mm and $cx = 1600$ mm) and for two distances between the sensor pair and the crack: 50 mm (Fig. 15(a)) and 225 mm (Fig. 15(b)). These results are obtained for the oscillation frequency $f = 2.5$ Hz and amplitude $\alpha = 2°$.

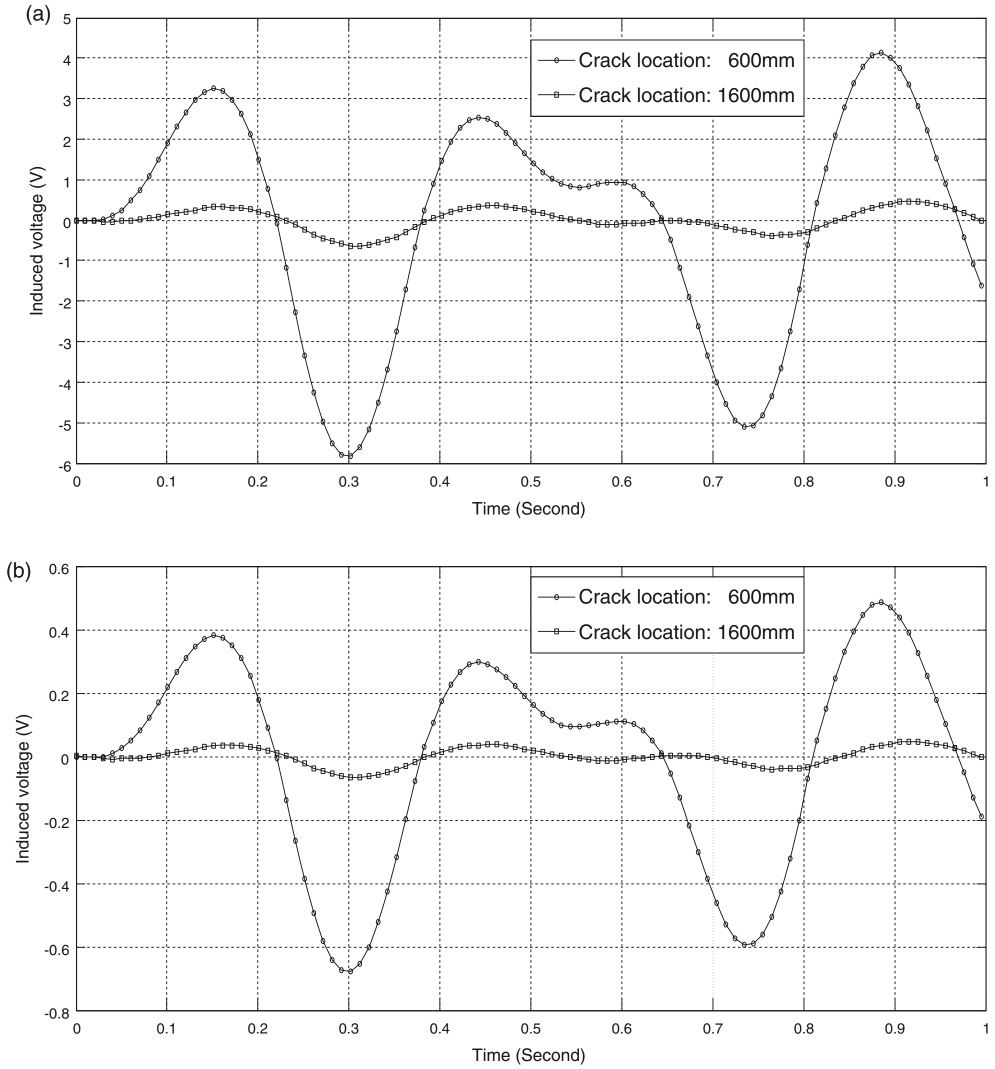

Fig. 15 Wing structure executing pitching oscillations: typical time variation of the voltage difference for two distances between the piezoelectric sensor pair and the crack: (a) 50 mm; (b) 225 mm ($f = 2.5$ Hz, $\alpha = 2°$)

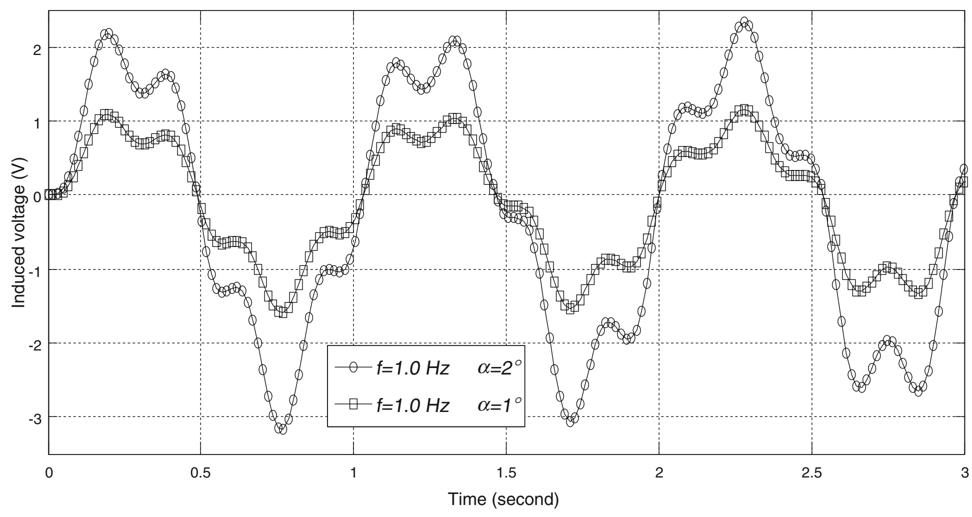

Fig. 16 Wing structure executing pitching oscillations: typical variation of the voltage difference with the amplitude of oscillation ($f = 1$ Hz, $\alpha = 1°$ and $2°$)

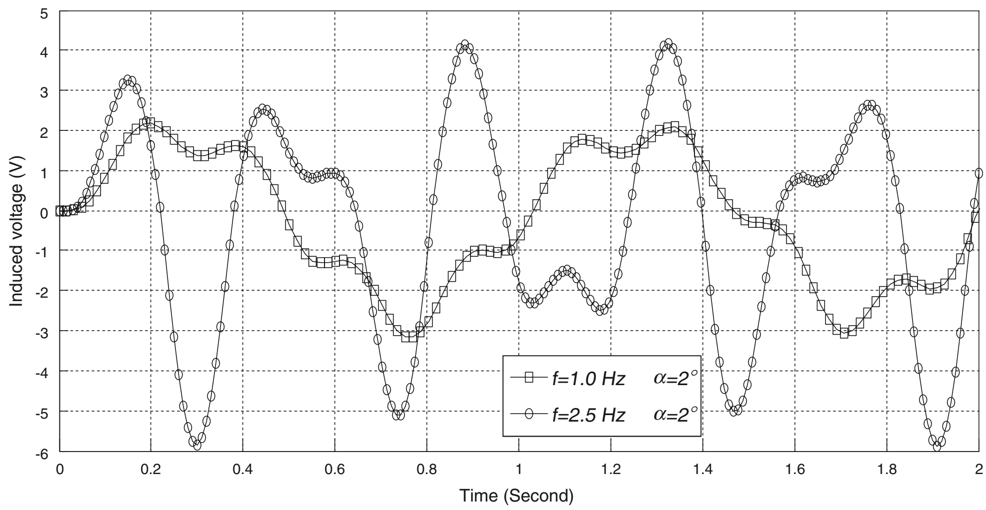

Fig. 17 Wing structure executing pitching oscillations: typical variation of the voltage difference with the oscillation frequency ($f = 1$ and 2.5 Hz, $\alpha = 2°$)

One can notice that in this case of pitching oscillations of the wing, the distance between the crack and the sensor pair for efficient crack detection is much improved in comparison with the steady case.

The effect of the amplitude of oscillation α and that of the oscillation frequency f on the voltage difference output of the piezoelectric pair are shown in Figs 16 and 17 for a distance between the crack and the sensor pair of 50 mm (the crack and sensor locations are cx = 600 mm and px1 = 550 mm). One can notice a significant increase of the differential voltage output with the increase in the oscillation amplitude or frequency.

6 CONCLUSIONS

This article presents a method using pairs of piezoelectric strip sensors bonded on thin structures with flexural deformations to detect the presence of cracks. Each pair of sensors consists of two piezoelectric strips bonded on the opposite sides of the structure at the same location. The measured voltage difference between the two piezoelectric strip sensors of a pair is proportional to the differential strain changes due to the presence of the crack. This method eliminates thus the need to know *a priori* the strains in the undamaged structure in order to predict the existence of a crack.

This method is used for thin structures executing flexural oscillations, in which case the cracks have a non-linear mechanical behaviour during the oscillatory cycle, by opening during the local extension phase and remaining closed during the local compression phase. This non-linear mechanical behaviour of the crack increases substantially the sensitivity of this crack detection method, permitting the detection of a crack situated relatively far from the piezoelectric sensors.

The dynamic response of the cracked structure is computed using a finite-element formulation of the piezoelectric strips coupled with the structure. A non-linear model is used for the crack with different mechanical behaviour of the crack in compression and extension. A panel method is used for the calculation of the unsteady aerodynamic loading acting on the oscillating wing structure.

The analysis of the structure with piezoelectric strips subjected to static loads has shown that the sensitivity of the piezoelectric sensor pair decreases substantially with the increase in the distance between the sensor and the crack.

The dynamic analysis in the frequency domain has shown that the voltage difference can have peak values large enough to be measured. These peak values are observed when the excitation frequencies are equal or close to the higher natural frequencies of the structure.

Compared to other methods, the dynamic analysis in the time domain has certain advantages. Large voltage differences can be obtained by using forced vibrations. If the damping is small, low excitation frequencies are more convenient for crack detection. The output value of the voltage difference increases with the crack depth and has an asymmetric shape when the sensor is not very far from the crack, thus increasing the detection efficiency.

The vibrations of a wing-like structure with bonded piezoelectric sensor pairs and subjected to steady and unsteady aerodynamic loads have also been studied for crack detection. It was found that the crack detection sensitivity is much improved in the case of unsteady aerodynamic loads when the wing-like structure executed flexural oscillations. The flexural oscillations of the wing structures may occur during certain flight evolutions, which may suggest that this crack detection approach could be used during the aircraft flight.

ACKNOWLEDGEMENTS

The financial support of the Natural Sciences and Engineering Research Council of Canada and of the Consortium for Research and Innovation in Aerospace in Quebec (CRIAQ) is gratefully acknowledged.

REFERENCES

1 **Doebling, S. W., Farrar, C. R.,** and **Prime, M. B.** A summary review of vibration-based damage identification methods. *Shock Vib. Dig.*, 1998, **30**, 91–105.
2 **Sohn, H., Farrar, C. R., Hemez, F. M., Shunk, D. D., Stinemates, D. W.,** and **Nadler, B.** A review of structural health monitoring literature: 1996–2001. Los Alamos National Laboratory report, LA-13976-MS, 2003.
3 **Masson, P., Micheau, P., Pasco, Y., Thomas, M., Brailoski, V., Meunier, M., Peter, Y.-A., Mateescu, D., Misra, A., Mrad, N., Pinsonnault, J.,** and **Cambron, A.** Smart technologies for structural health monitoring of aerospace structures. In Proceedings of the Cansmart 2006 International Workshop, Smart Materials and Structures, Toronto, ON, Canada, October 2006, pp. 1–12.
4 **Rees, D., Chiu, W. K.,** and **Jones, R.** A numerical study of crack monitoring in patched structures using a piezoelectric sensor. *Smart Mater. Struct.*, 1992, **1**, 202–205.
5 **Kwon, Y. W.** and **Lannamann, D. L.** Dynamic numerical modeling and simulation of interfacial cracks in sandwich structures for damage detection. *J. Sandwich Struct. Mater.*, 2000, **4**, 175–199.
6 **Lingyu, Yu.** and **Giurgiutiu, V.** Multi-mode damage detection methods with piezoelectric wafer active sensors. *J. Intell. Mater. Syst. Struct.*, 2009, **20**, 1329–1341.
7 **Giurgiutiu, V.** and **Rogers, C. A.** Modeling of the electromechanical impedance response of a damaged composite beam. In Proceedings of the ASME Winter Annual Meeting, Aerospace and Materials Divisions, Adaptive Structures and Material Systems Symposium, Nashville, TN, 2000, AD-Vol. 87, pp. 39–46.
8 **Zagrai, A. N.** and **Giurgiutiu, V.** Electro-mechanical impendance method for crack detection in thin plates. *J. Intell. Mater. Syst. Structs*, 2001, **12**, 709–718.
9 **Liu, W. P.** and **Giurgiutiu, V.** Finite element simulation of piezoelectric wafer active sensors based structural health monitoring. In Proceedings of the ASME 2007 International Mechanical Engineering Congress and Exposition (IMECE2007), Seattle, Washington, November 2007, pp. 715–726.
10 **Liu, T., Martin, V.,** and **Kitipornchai, K.** Modelling the input–output behaviour of piezoelectric structural health monitoring systems for composite plates. *Smart Mater. Struct.*, 2003, **12**, 836–844.
11 **Li, Y. Y., Cheng, L. H., Yam, L. H.,** and **Yan, Y. J.** Numerical modeling of a damaged plate with piezoelectric actuator. *Smart Mater. Struct.*, 2003, **12**, 524–532.
12 **Wang, Q., Quek, S. T.,** and **Liew, K. M.** On the repair of a cracked beam with a piezoelectric patch. *Smart Mater. Struct.*, 2002, **11**, 404–410.
13 **Sinha, J. K., Friswell, M. I.,** and **Edwards, S.** Simplified models for the location of cracks in beam structures using measured vibration data. *J. Sound Vib.*, 2002, **251**(1), 14–38.
14 **Lee, C.-K., Chiang, W.-W.,** and **O'Sullivan, T. C.** Piezoelectric modal sensors and actuators achieving critical damping on a cantilever plate. In Proceedings of the AIAA/ASME/ASCE/AHS/ASC 30th Structures, Structural Dynamics and Materials Conference, Mobile, Alabama, USA, April 1989, pp. 2018–2026.
15 **Van Popel, J.** and **Misra, A. K.** Active control of space structures using bonded piezoelectric film actuators. In Proceedings of the AIAA/AAS Astrodynamics Conference, Hilton Head Island, SC, 1992, pp. 328–341.
16 **Venneri, S. L.** and **Wada, B. K.** Overview of NASA's adaptive structure program. In Proceedings of the 44th Congress of the International Astronautical Federation, Austria, 1993, pp. 1–13.
17 **Mateescu, D., Misra, A. K.,** and **Shrivastava, S.** Aeroelastic oscillations of a delta wing with piezoelectric strips in supersonic flow. *Math. Engng Sci. Aerosp.* (*Cambridge Sci. Pub. J.*), 2010, **1**(2), 119–138.
18 **Yang, Y., Ju, H. K.,** and **Soh, C. K.** Analytical and semi-analytical solutions for vibration control of a cantilevered column using a piezoelectric actuator. *Smart Mater. Struct.*, 2003, **12**, 193–203.
19 **Bruant, I., Coffignal, G., Lene, F.,** and **Verge, M.** Active control of beam structures with piezoelectric actuators and sensors: modeling and simulation. *Smart Mater. Struct.*, 2004, **10**, 404–408.
20 ANSYS Inc. *ANSYS Release 9.0 documentation*, 2004.
21 **Preumont, A.** *Vibration control of active structures-An introduction*, 1997 (Kluwer Academic Publishers, Dordrecht, The Netherland, Boston, USA).